Environmental Science
Processes & Impacts

Accepted Manuscript

ROYAL SOCIETY OF CHEMISTRY

rsc.li/process-impacts

Electrochemical Mineral Scale Prevention and Removal on Electrically Conducting Carbon Nanotube – Polyamide Reverse Osmosis Membranes

Wenyan Duan, Alexander Dudchenko, Elizabeth Mende, Celeste Flyer, Xiaobo Zhu, David Jassby
Department of Chemical and Environmental Engineering, University of California, Riverside
900 University Ave., Riverside, CA 92521, USA. E-mail: djassby@engr.ucr.edu; Fax: +1 (951) 827 5696; Tel: +1 (951) 827 6475

Abstract

The electrochemical prevention and removal of $CaSO_4$ and $CaCO_3$ mineral scales on electrically conducting carbon nanotube – polyamide reverse osmosis membrane was investigated. Different electrical potentials were applied to the membrane surface while filtering model scaling solutions with high saturation indices. Scaling progression was monitored through flux measurements. $CaCO_3$ scale was efficiently removed from the membrane surface through the intermittent application of a 2.5 V potential to the membrane surface, when the membrane acted as an anode. Water oxidation at the anode, which led to proton formation, resulted in the dissolution of deposited $CaCO_3$ crystals. $CaSO_4$ scale formation was significantly retarded through the continuous application of 1.5 V DC to the membrane surface, when the membrane was operated as an anode. The continuous application of a sufficient electrical potential to the membrane surface leads to the formation of a thick layer of counter-ions along the membrane surface that pushed $CaSO_4$ crystal formation away from the membrane surface, allowing the formed crystals to be carried away by the cross-flow. We developed a simple model, based on a modified Poisson-Boltzmann equation, which qualitatively explained our observed experimental results.

Introduction

Desalination is an increasingly used method to provide potable water to areas with limited fresh water resources.[1, 2, 3] However, this technology is still plagued by several issues, principal amongst them is membrane fouling.[4, 5, 6] State-of-the-art commercial revers osmosis (RO) membranes operate near the thermodynamic limit.[7] Therefore, to improve membrane performance and reduce process energy consumption, pretreatment and membrane fouling reduction must be achieved.[2] One type of membrane fouling process is mineral scaling, where salt crystals precipitate out of the solution, forming a dense layer on the membrane surface that obstructs the flow of water through the membrane. Mineral scaling occurs when the concentration of rejected ions along the membrane surface exceeds the solubility limit for a particular mineral, resulting in the nucleation and growth of inorganic crystals on the membrane surface.[8, 9, 10] The phenomenon where a layer of ions accumulates along the membrane surface is known as concentration polarization (CP). Once scaling occurs, the RO system will experience a significant decrease in water flux and could be physically damaged, which could lead to a drop in salt rejection.[11] Additionally, the nucleated salt crystals can physically harm the membrane surface. Depending on salt crystal species, mineral scaling can be controlled in RO membrane systems by using turbulent flow conditions that enhance mixing in the feed solution and reduce solute concentrations along the membrane surface, through the addition of anti-scaling chemicals, by adjusting the solution pH[12, 13, 14], or by some combination of the above. Two of the most common mineral species responsible for mineral scale formation in membrane applications are $CaCO_3$ and $CaSO_4$.[12, 14] $CaCO_3$ scale can be controlled by adjusting solution pH, as $CaCO_3$ dissolves readily under acidic conditions.[12] In contract, $CaSO_4$ is pH insensitive, and requires the addition of anti-scaling agents.[15]

Mineral scaling formation has been studied for decades, with two main mechanism identified: homogeneous crystal growth occurs when salt crystals form and grow in the solution and heterogeneous crystal growth on a solid surface (such as a membrane surface).[9, 10, 16] In general, the heterogeneous route causes more rapid crystal formation and growth. The growth rate of crystal depends on degree of super-saturation (expressed as the saturation index) as well as the local ratio of cations to anions.[17]

The accumulation of ions on the membrane surface and the formation of the CP layer are associated with diffusion and advection of ion toward, away from, and along the membrane surface. However, the application of an electric charge to a surface leads to the formation of an electrical double layer (EDL) along the surface.[18] In the EDL structure, the concentrations of co-ions and counter ions are non-stoichiometric, with counter ion

concentrations decreasing and co-ions concentrations increasing as the distance from the charged surface grows, until bulk concentrations are achieved. The distance from the electrically charged surface where bulk concentrations exist is a function of the surface charge and solution ionic strength.[19, 20, 21] Several reports have demonstrated that excess concentrations of either anions or cations lead to delayed nucleation and crystal growth, with the most rapid crystal growth observed when stoichiometric conditions exist.[21, 17]

Several reports have demonstrated that the application of an electric field during cross-flow filtration reduces the impact of various fouling mechanisms, including CP formation and organic material deposition.[22, 23, 24, 25] We have developed an electrically conducting RO membrane that maintains the transport properties needed in desalination processes, with the added benefit of high electrical conductivity.[26] Electrical conductivity is imparted through the combination of functionalized carbon nanotubes (CNTs) that are cross-linked to the polyamide (PA) membrane matrix, forming a true nano-composite.

In this paper we describe how the application of an electrical potential to the surface of an electrically conducting RO membrane can significantly delay the formation of $CaSO_4$ crystals near on membrane and dissolve $CaCO_3$ crystals growing on the membrane surface. Furthermore, we develop a model that predicts the concentrations of ions as a function of applied membrane potential and distance from the membrane surface. We use this model to qualitatively explain the observed decline in $CaSO_4$ fouling.

Materials and Methods

A. Materials

Carboxylated multiwall carbon nanotubes (CNT-COOH) were purchase from Cheap Tubes (Cheaptubes inc., Brattleboro, VT). Polysulfone (PSF) ultrafiltration (UF) supports were purchased from Sepro Membranes (Sepro Membranes Inc., Oceanside, CA). M-phenylenediamine (MPD), trimesoyl chloride (TMC), $CaCl_2$, $NaSO_4$, $MgSO_4$, sodium dodecylbenzenesulfonate (NaDDBS), and $NaHCO_3$ were purchased from Sigma-Aldrich and used as received.

B. Membrane Fabrication

The RO membrane fabrication process followed our previously reported method.[26] In short, CNT-COOH suspensions were created by sonicating the CNT-COOH in a solution containing the surfactant NaDDBS for 30 minutes. Then, a certain volume of CNT-COOH suspension was deposited onto a PSF UF support, rinsed with deionized water (DIW), and allowed to dry. Then the support was immersed in a 2% aqueous solution of MPD for two hours, slightly dried, and immersed into a 0.15% solution of TMC in hexane for two minutes. The membranes were then cured for 10 minutes at 90°C and stored in DIW at 4°C until use.

C. Membrane Characterization

Scanning electron microscopy (SEM, JEOL Akishima-Shi, Tokyo) was used to image the surface morphology as well as the salt crystals growing on the membranes. For SEM images, the conducting nature of the membrane negated the need to sputter-coat the membrane with a metal layer. Attenuated total reflectance – Fourier transformed infracted spectroscopy (ATR-FTIR, Thermo Scientific, Franklin, MA) was used to verify the formation of ester bonds between CNT-COOH and the PA polymer matrix.[27] A four-point conductivity probe was used to characterize membrane sheet resistance. The open-circuit potential of the membrane, representing the "true" potential on the membrane surface, was measured in reference to a Ag/AgCl reference electrode using a potentiostat (Gamry Instruments, Warminster, PA).[28] Atomic force microscopy (AFM; Bruker Biosciences, Billerica, MA) was use to measure membrane surface roughness.

D. Experimental Procedure

A modified cross-flow RO module was used in all scaling experiments; the module incorporates electrodes designed to deliver an external charge to the membrane surface and a counter electrode (316 stainless steel sheet) seated 3 mm above the membrane surface. The electrodes delivering the external charge are positioned outside of the inner O-ring, and do not come into contact with the solution. The active membrane area in this setup was 20 cm^2 (4.8 cm × 4.2 cm).

The feed solution was continuously re-circulated though the system (Figure S1), and the permeate was weighed periodically to determine flux. The system was operated in a constant pressure mode, with the initial pressure adjusted so as to maintain identical initial flux values for all experiments. Pressure was controlled by adjusting a needle valve on the retentate line, and a diaphragm pump was used to provide flow and pressure to the system (Wanner Engineering, Minneapolis, MN). External electrical potentials were applied to the membrane surface by connecting the membrane to an arbitrary waveform generator (Rigol, Oakwood Willage, OH). Permeate quality was continuously monitored by measuring its conductivity.

E. $CaSO_4$ Scaling Experiments

In these experiments, we used a scaling solution meant to simulate brackish groundwater (Table 1).[29]

Table 1 $CaSO_4$ Scaling Experiments Salt Composition

Salt	Concentration (M)
Na_2SO_4	0.0105
$MgSO_4$	0.0145
$CaCl_2$	0.0164

A large volume (4 L) of the scaling solution (saturation index of 1.01 with respect for $CaSO_4$) was continuously recycled through the system with no crystal formation observed in the bulk. In some of the $CaSO_4$ scaling experiments, an in-line 0.5 μm polycarbonate filter was used on the retentate line to trap any crystals formed during the filtration experiments. [29] In these experiments the cross-flow velocity in the RO module was maintained at either 3.4 cm/s, when the in-line filter was used, or 4.5 cm/s when no in-line filter was present. The increased flow rate associated with the higher velocities resulted in a transmembrane pressure across the in-line filter that exceeded the filter housing's capacity and led to leaks. A DC voltage was continuously supplied to the membrane surface, with the membrane acting as an anode with an applied potential of 1.5V (approximately 1 V vs. a Ag/AgCl reference electrode).

F. $CaCO_3$ Scaling Experiments

In these experiments, we used a scaling solution described in Table 2.[30]

Table 2 $CaCO_3$ Scaling Experiments Salt Composition

Salt	Concentration (M)
Na_2CO_3	0.0094
KCl	0.0107
$CaCl_2$	0.0072
$MgCl_2$	0.0047

The scaling solution (saturation index of 4.38 with respect for $CaCO_3$) was continuously recycled through the system without filtration. No crystal formation was observed in the bulk. In these experiments, the cross-flow velocity in the RO module was maintained at 4.5 cm/s. The membranes were allowed to scale for a period of several hours, and then a 2.5V potential (membrane as anode) was applied for 15 minutes. After that, the voltage was shut off and the system was allowed to continue operating.

Results and Discussion

A. Membrane Characterization

The electrically conducting RO membrane achieved a NaCl rejection rate of 98% (tested using an 8 g/L NaCl solution). Pure water flux was determined to be 2 ± 0.53 LMH/bar. This value is somewhat lower than that reported from commercial RO membranes (typical values of pure water flux ranging between 3.2-3.96 LMH/bar), but hardly surprising as we did not subject our membranes to any post-fabrication processing steps used to enhance membrane flux.[31] It is important to note that the application of an electrical potential did not change salt rejection or pure water flux through the membrane. SEM images of the membrane surface show the typical "noodle" structure associated with PA RO membranes (Figure 1 Left).

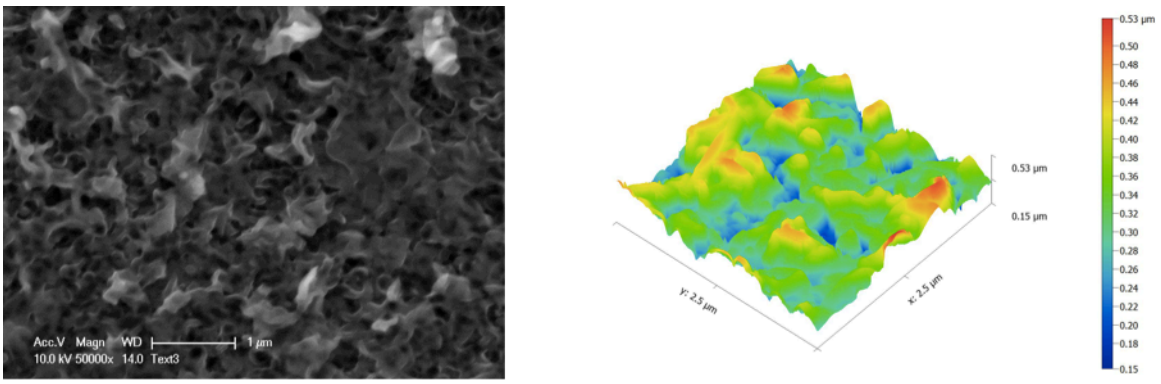

Figure 1. (Left) SEM image of surface of PA-CNT RO membrane; (Right) AFM map shows roughness according to the software RMS is 91nm on 2.5 by 2.5µm spot.

Sheet resistance was measured to be 2.56±0.71 kΩ. An AFM image of the membrane surface can be seen in Fig. 1 (Right). AFM image analysis indicated that membrane surface roughness was 91 nm. This roughness value is similar to values reported in previous studies of RO membrane surface.[32, 33] ATR-FTIR analysis of the membrane surface revealed the presence of an ester bond (1728 cm-1) linking the hydroxyl group on the CNTs to the TOC monomer in the PA, as well as the characteristic peaks corresponding to the amide bonds linking the TMC and MPD monomers (1643 cm-1, 1610 cm-1, and 1543 cm-1; Figure 2).[26]

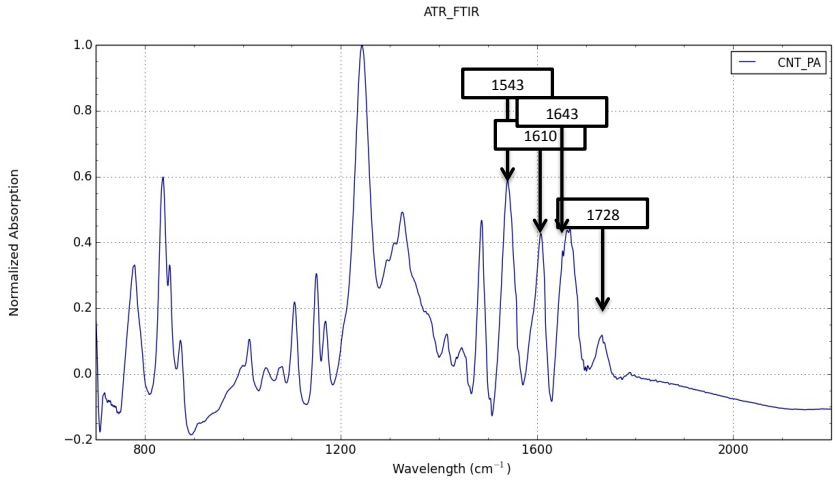

Figure 2. ATR-FTIR spectra of the electrically conducting RO membrane

The open circuit potential of the membrane as a function of the applied potential can be seen in Fig. S2; this potential represents the approximate potential (as there will be some potential drop between the membrane and reference electrode), with reference to the Ag/AgCl electrode, that the solution around the membrane experiences. The ionic strength of the solution was 164 mM and the distance between the working and reference electrode was 5 mm. Thus, when a potential of 2.5V is applied to the membrane/counter electrode pair and the membrane is used as an anode, the "true" potential on the membrane surface will be approximately 1.8V vs. the Ag/AgCl reference; this potential (which is 1.23 V for the water-splitting reaction vs. the hydrogen standard electrode) is sufficient to spilt water and produce protons along the membrane surface.[34]

B. $CaCO_3$ Scaling Removal

In this portion of the study we demonstrate the ability of the electrically conducting RO membrane to remove $CaCO_3$ scale that grew on the membrane surface during the treatment of brackish water with a high

saturation index with respect to $CaCO_3$ (Table 2). The growth of $CaCO_3$ scale on the membrane surface results in a significant drop in flux (Figure 3). Flux recovery was consistently demonstrated upon the application of an external potential to the membrane surface, when the membrane was used as an anode.

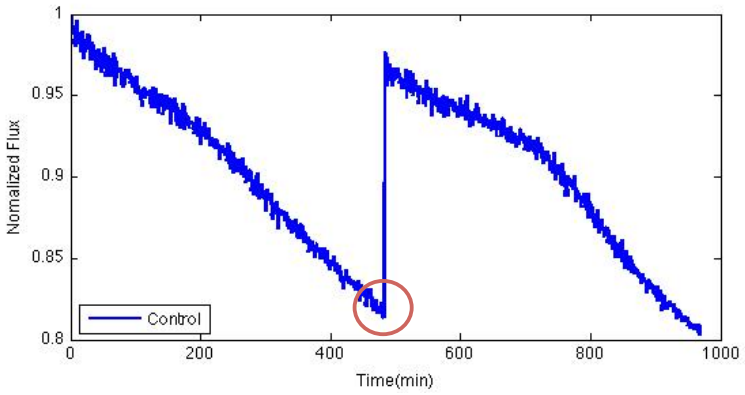

Figure 3. $CaCO_3$ scaling experiment; flux declined as $CaCO_3$ scale developed on the membrane surface. When a 2.5V potential (designated by a red circle) was applied (membrane as anode), and the membrane was flushed at high velocities, flux was fully recovered.

As shown in Fig. 3, when no electrical potential was applied to the membrane surface the flux through the membrane experienced a persistent drop as a result of the growth of $CaCO_3$ scale, with water fluxes declining by over 18% over a period of 460 minutes. After ~460 minutes, the pressure was shut off and a 2.5V potential was applied to the membrane/counter electrode pair for 30 minutes (5 min. on/5 min. off). As can be seen, the water flux quickly recovered to near (98% recovery) the initial value, indicating that the $CaCO_3$ scale was effectively removed from the membrane surface. After 30 minutes, the potential was shut off and the pressure resumed, and the system experienced resumed fouling due to $CaCO_3$ scaling. These results were observed in multiple experiments, and can be seen in the Supporting Information (Figures S5-S7). Simple flushing of the membrane (with no potential applied) did not result in any flux recovery. The reason the pressure was turned off during the application of the potential was the need to increase cross-flow velocities during the descaling process. The diaphragm pump used during the pressurized mode could only deliver a velocity of 4.5 cm/s; at these flow velocities, any detached CaCO3 scale quickly re-deposited on the membrane surface. To avoid this, we used a peristaltic pump, which delivered a flow velocity of 8.6 cm/s, during the de-scaling stage. At this velocity, the detached $CaCO_3$ was quickly removed from the system and flux was rapidly restored.[10] While the flow velocities provided by the peristaltic pump were higher, they were still very low and in line with flow velocities used in many RO processes. Visual inspection of the membrane before and after the electrical de-scaling treatment clearly demonstrated the impact of the applied voltage, with the electrified membrane exhibiting a significantly reduced white area corresponding to the presence of $CaCO_3$ crystals (Figure. 4).

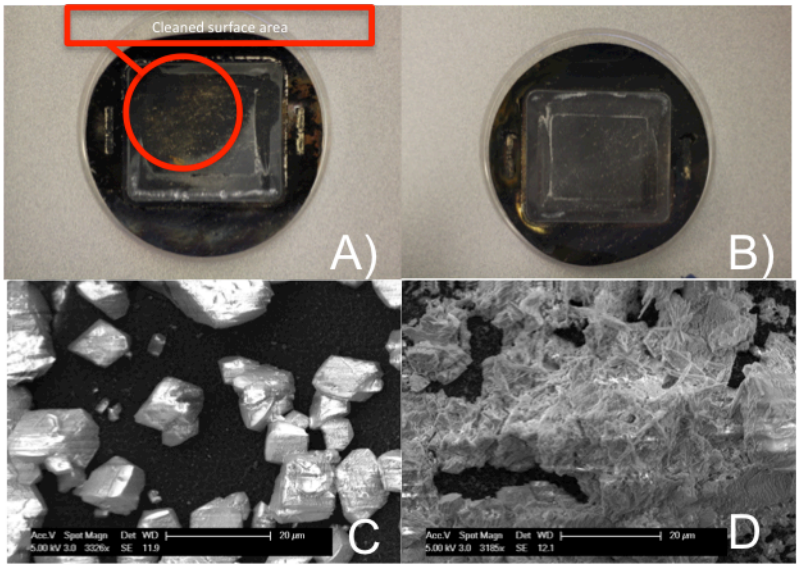

Figure 4. A) Electrically conducting RO membrane surface area after the application of 2.5V; the white area, corresponding to areas still covered by $CaCO_3$ is greatly reduced; B) Membrane area fully covered by $CaCO_3$ scale; C) SEM of membrane surface after the application of 2.5V displaying few $CaCO_3$ crystals; D) Thick $CaCO_3$ deposits on fouled membrane surface (no voltage applied).

As displayed in Fig. S2, the "true" potential on the membrane when 2.5V are applied to the membrane/counter electrode pair (when the membrane is used as an anode) is 1.8V vs. the Ag/AgCl reference electrode. At this potential water oxidation occurs, and results in the formation of H^+ along the membrane surface (membrane as anode).[31]

$$2\ H_2O(l) \rightarrow O_2(g) + 4\ H^+(aq) + 4e^-$$

The corresponding half reaction takes place on the cathode

$$4\ H^+(aq) + 4e^- \rightarrow 2H_2(g)$$

$CaCO_3$ crystals are very pH sensitive, and dissolve rapidly in low pH conditions.[31, 12] Thus, when the electrical potential is applied to the scaled membrane surface local pH values are reduced due to the formation of H^+, and the deposited $CaCO_3$ crystals dissolve/detach from the membrane surface, resulting in flux restoration.

C. $CaSO_4$ Scale Prevention

Here we demonstrate the ability of the electrically charged membrane to significantly delay the onset of $CaSO_4$ scale formation. In contrast to $CaCO_3$, $CaSO_4$ scale is pH insensitive, and cannot be removed through pH adjustments. As in the case of $CaCO_3$ scaling, the growth of CaSO4 scale on the membrane surface is associated with flux decline and performance loss. We investigated two scenarios in this portion of the study; in the first scenario, the $CaSO_4$ scaling solution was recycled through the RO module with no filtering and in the second scenario we added an in-line 0.5µm microfilter designed to remove any particulate $CaSO_4$ formed during the experiment and carried along the feed stream.

When no in-line filter was used, the continuous application of 1.5V to the membrane/counter electrode pair (membrane as anode) led to a slight decline in the rate of flux decay (Figure 5). These results were done in duplicate and can be seen in the Supporting Information.

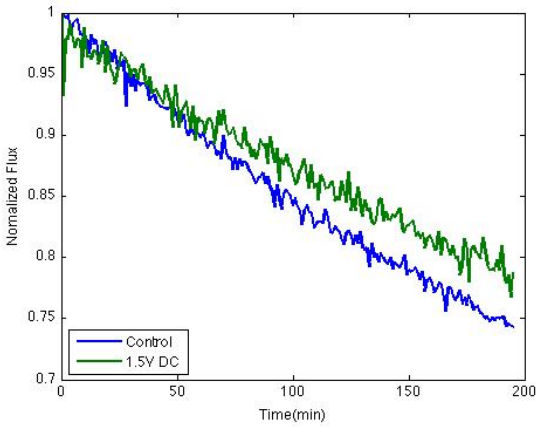

Figure 5. Flux decline due to $CaSO_4$ scaling with no in-line filter; membrane was used as an anode with a cross-flow velocity of 4.5 cm/s.

When no potential was applied, the rate of flux decline was 30% greater than the flux decline rate experienced by the electrically charged membrane. When an in-line filter was used, the rate of flux decline experienced by the non-charged membrane was more than twice that experienced by the electrically charged membrane (1.5V as anode) (Figure 6). Duplicates of these experiments can be seen in the supporting information (Figure S3 and S4).

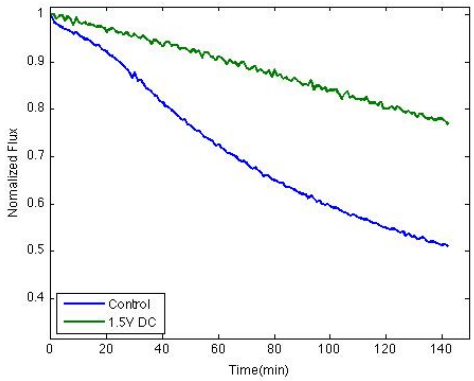

Figure 6. Flux decline due to $CaSO_4$ scaling with in-line 0.5 µm filter and a cross-flow velocity of 3.4 cm/s.

This would indicate that a large amount of flux decline observed when no in-line filter was used could be associated with secondary deposition of $CaSO_4$ crystals formed during the RO process. Indeed, after prolonged use, the in-line filter developed a coarse yellowish coating, which we assumed to be trapped $CaSO_4$ crystals formed during the RO process. In a typical RO system, the feed stream would not be recycled. There fore, the in-line filtration conditions are more representative of realistic conditions one would encounter in field applications of RO technology. Membrane fouling rates in the absence of the inline filter are similar to the flux decline observed when an in-line filter was used and the membrane was electrically charged. However, flow velocities used when the in-line filter was present were significantly lower than those used when the filter was absent, which would lead to more challenging fouling conditions.

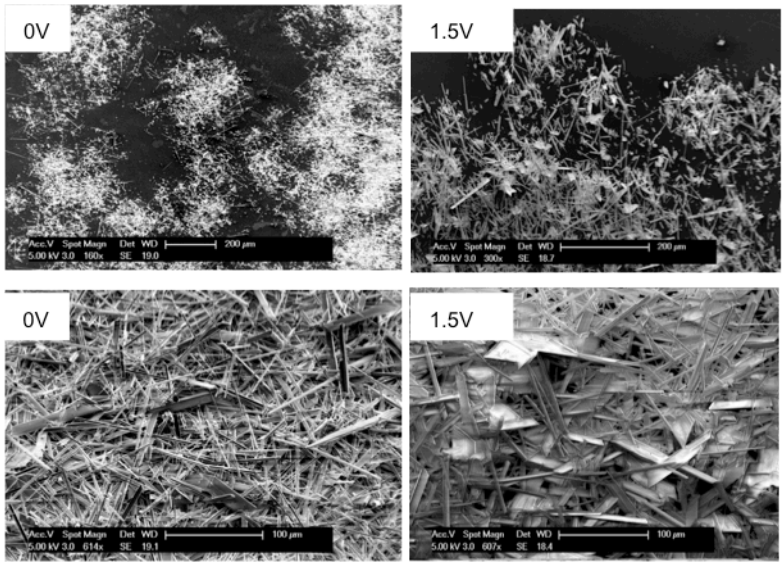

Figure 7. SEM images of the membrane surface covered by $CaSO_4$ crystals; CaSO4 scale morphology changes as a function of the applied potential. Top images are from the "transition" zone and bottom images are from the main part of the membrane (see Figure S8 in the supporting material for a detailed description of membrane zones).

Applying a positive external charge to the membrane surface also had a significant impact on the deposited crystal morphology. When no voltage was applied, the $CaSO_4$ exhibited the typical needle-like morphology, and the crystals were tightly packed (Figure 7). In contrast, When the membrane is used as an anode with 1.5 V applied, we can see that the crystals are much larger, and not as tightly packed, which would explain why the flux decline was not as severe, as water can flow through the scale structure.

When an electrically charged surface is placed in contact with an ionic solution, ions will redistribute themselves to maintain system electroneutrality, forming an EDL.[18, 20] Thus, when the membrane is positively charged (membrane as anode), negative counter ions will flock to the membrane surface, while positive co-ions will be repelled away from the membrane; along the counter electrode (cathode) the situation is reversed. The number of counter-ion associated charges (negative charges when membrane is used as anode) along the membrane surface will equal the number of positive charges on the membrane surface; the number of positive charges on the membrane surface is proportional to the membrane electrical potential. Thus, by applying high external potentials to the electrically conducting RO membrane surface, large numbers of negative counter ions are needed along the membrane surface to maintain electroneutrality.

Due to the hydrated volume of counter-ions, when a sufficiently charged membrane surface is brought into contact with an ionic solution, a single layer of ions will not be sufficient to ensure charge neutrality. Thus, multiple layers of counter-ions accumulate along the membrane surface.[19, 35] In these layers, the concentration of co-ions are near zero. For rapid nucleation to occur, both positive and negative ions need to be present in near-equal concentrations.[17, 21] Therefore, in the presence of a highly charged surface, the nucleation of sparingly soluble salts, such as $CaSO_4$, is discouraged near the charged surface. Away from the charged membrane surface the concentrations so f co- and counter-ions equalize, and rapid nucleation can take place. However, the crystal nuclei are formed away from the membrane surface, and can be carried away by the cross-flow.

D. Modelling Ion Concentrations Along an Electrically Charged RO Membrane Surface

The standard Poisson-Boltzmann (SPB) model can be used to predict ion concentrations near a charged surface when surface potentials do not exceed ~ 200 mV.[36] However, when surface potentials exceed 200 mV, the basic assumption on which the SPB model is based is violated, namely that the ions are in an infinitely dilute solution. The SPB model does not take into account the finite volume of ions, and therefore has no limit to the number of counter ions in the Stern layer, which is physically impossible. One result of this over-simplification is that the SPB over predicts the potential drop as one moves away from the charged surface. A

useful modification to the SPB model, known as the modified PB model (MPB), considers the volume of ions when calculating the number of counter-ions attracted to an oppositely charged surface. As a result, the MPB equation predicts a region along the membrane surface, that is more than one molecule thick, where only counter ions exist; this layer is significantly thicker than the single layer of counter ions in the Stern layer used by in the SPB model.

We used the MPB model to predict the potential as a function of distance from the membrane surface (Figure 8 A) [37]:

$$\varepsilon_e \frac{d^2\Psi}{dx^2} = \frac{-eN_A \sum_{i=1}^{m} z_i c_i^{\infty} \exp\left(-\frac{z_i e\Psi}{kT}\right)}{1+\sum_{i=1}^{m} \frac{c_i^{\infty}}{c_i^{\max}}\left[\exp\left(-\frac{z_i e\Psi}{kT}\right)-1\right]}$$

We then used the predicted potential to calculate the local ion concentrations as a function of distance from the membrane [37]:

$$c_i = \frac{c_i^{\infty} \exp\left(-\frac{z_i e\Psi}{kT}\right)}{1+\sum_{i=1}^{m} \frac{c_i^{\infty}}{c_i^{\max}}\left[\exp\left(-\frac{z_i e\Psi}{kT}\right)-1\right]}$$

where ψ is the electrical potential, z is the valence of ions, e is the elementary charge, N_A is Avogadro's number, c_i^{∞} is the bulk ion concentration, c_i^{max} is the maximum ion concentrations in a given space given ionic steric effects, ε_e is the permittivity of the electrolyte solution (changes with ion concentration), k is Boltzmann's constant, and T is temperature. The boundary conditions for this problem are $\psi_{x=0} = \psi_{applied}$ and $\psi_{bulk} = 0$. c_i^{max} can be calculated using the following equation [37]:

$$c_i^{\max} = \frac{p}{\frac{4}{3}\pi R_i^3 N_A}$$

where p is a packing coefficient, R_i is the ionic radius, and N_A is Avogadro's number.

We used these equations to predict the concentrations of Ca^{2+} and SO_4^{2-} ions as a function of distance from the membrane surface. In this model, we used the Ca^{2+} and SO_4^{2-} concentrations found in our model $CaSO_4$ scaling solution (Table 1). As expected, the model predicted that by increasing the applied electrical potential to the membranes surface (membrane as anode) the layer of SO_4^{2-} counter-ions extends further away from the membrane surface (Figure 8 B). When modelling the system, we did not consider the concentration polarization (CP) layer formed along the membrane surface. As can be seen in Fig. 8 B and 8 C, the concentrations of counter-ions (SO_4^{-2}) along the membrane surface reached a maximum of approximately 4.6 M. This maximum concentration is a function of the volume of the hydrated ions, and as can be seen, this value is reached when 250 mV are applied to the membrane surface; increasing the applied surface potential simply expands the counter-ion exclusive zone but does not increase the maximum ion concentration, which is physically bound. Beyond the exclusive counter-ion zone, the concentrations of counter- and co-ions begin to converge, eventually reaching the concentration within the CP layer. We do not consider ion concentration change from the bulk to the CP in this model, as it does not impact ion concentrations within the first few nm away from the membrane, which are wholly dependent on the surface potential.

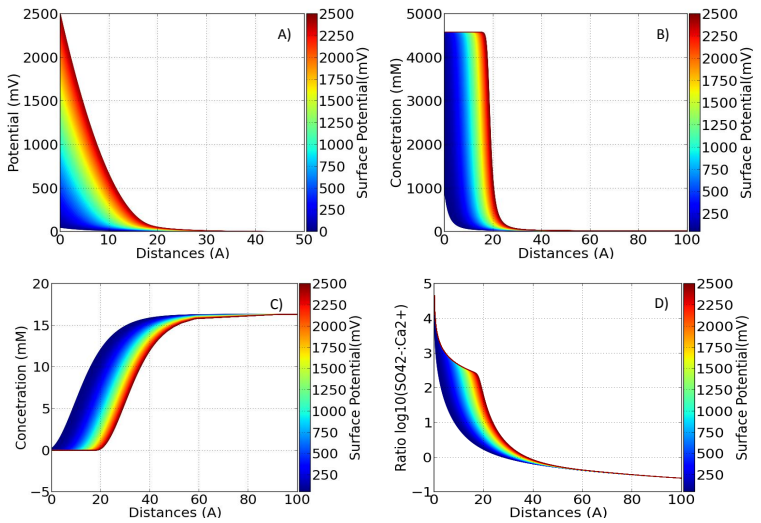

Figure 8. MPB model results; A) potential drop as a function of membrane surface potential and distance from the membrane surface; B) Concentrations of SO_4^{-2} ions as a function of membrane surface potential and distance from membrane surface. C) Concentration of Ca^{+2} ions as a function of membrane surface potential and distance from membrane; D) ratios between SO_4^{-2} and Ca^{+2} ions as a function of surface potential and distance from the membrane surface

Correspondingly, the distance away from the membrane where Ca^{2+} ions are excluded grows (Figure 8 C). The ratio between Ca^{2+} and SO_4^{2-} ion concentrations, which determines the nucleation rate of $CaSO_4$, demonstrates that as the membrane electrical potential increases from zero to 2.5V, the distance from the membrane where stoichiometric concentrations exist more than doubles, from below 2 nm to more than 4 nm (Figure 8 D). Thus, the region where nucleation can actually take place is pushed out away from the membrane surface, which would reduce the ability of the formed $CaSO_4$ nuclei to attach and grow on the membrane surface (Figure 9). While these distances are very small, it is important to remember that the size of a $CaSO_4$ crystal nucleus is approximately 1.5 nm. Therefore, the nucleus does not form directly near the membrane surface, and can be carried away by the cross flow.

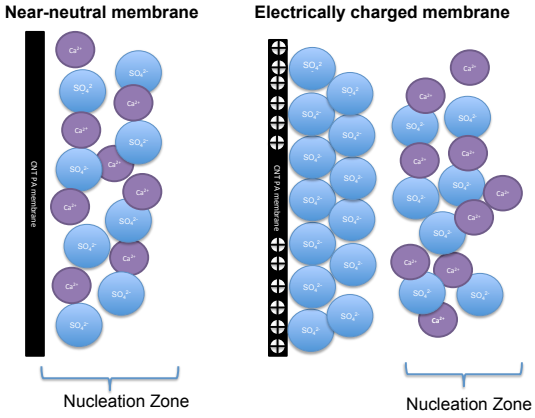

Figure 9. As the applied surface potential increases, the region near the membrane where only SO_4^{2-} ions exist expands out into the solution, which pushes the nucleation zone away from the membrane surface.

The surface roughness of the electrically conduction RO membrane used in this study was determined to be 91 nm (Figure 1). Thus, in our experimental system, when a crystal is formed in a membrane "crevice" it is less likely to be carried away by the cross-flow as opposed to a crystal formed on a "hill" where the cross-flow is more likely to remove the crystal. The model qualitatively explains our experimental observations: the application of an external potential to the membrane surface leads to a decrease (but not outright prevention) in

membrane scaling rates. We hypothesize that by reducing membrane surface roughness we will be able to eliminate membrane areas that are likely to "trap" crystal nuclei, thus improving membrane performance.

Conclusion

In this paper we describe how the application of an electrical potential to the surface of an electrically conducting CNT-PA composite RO membrane can remove $CaCO_3$ scale and significantly slow the formation of $CaSO_4$ scale. When the membrane is used as an anode, the application of 2.5V leads to the formation of localized H^+ due to the oxidation of water, which cause the dissolution and removal of $CaCO_3$ scale deposited on the membrane surface. $CaSO_4$ scale growth, which is pH-insensitive, was significantly delayed through the application of relatively low electrical potentials to the membrane surface (1.5V, which is below the water splitting point). We used as MPB model to predict ion concentrations along the membrane surface as a function of the applied electrical potential; when sufficient electrical potential was applied, the ratio between anions and cations was altered, which has been shown to lead to a drop in crystal nucleation rates. Crystals that did form did so away from the membrane surface and were carried away by the cross-flow, which we hypothesize is the reason for the observed drop in $CaSO_4$ fouling rates. The results of this study illustrate the potential benefits of using electrically conducting membranes in RO water treatment processes. Widespread adoption of this technology could significantly reduce the use of anti-scaling chemicals and acids in the treatment of brackish groundwater and recycled wastewater.

Acknowledgements

Financial support for this study was provided by the University of California at Riverside.

References

1. M. a Shannon, P. W. Bohn, M. Elimelech, J. G. Georgiadis, B. J. Mariñas, and A. M. Mayes, *Nature*, 2008, **452**, 301–10.

2. M. Elimelech and W. Phillip, *Science*, 2011, **333**, 712–717.

3. J. Yeston, R. Coontz, J. Smith, and C. Ash, *Science* , 2006, **313** , 1067.

4. B. Van Der Bruggen, C. Vandecasteele, T. Van Gestel, W. Doyen, and R. Leysen, *Environmental Progress*, 2003, **22**, 46–56.

5. K. L. Chen, L. Song, S. L. Ong, and W. J. Ng, *Journal of Membrane Science*, 2004, **232**, 63–72.

6. H. K. Lonsdale, *Journal of Membrane Science*, 1982, **10**, 81–181.

7. A. Zhu, A. Rahardianto, P. D. Christofides, and Y. Cohen, *Desalination and Water Treatment*, 2010, **15**, 256–266.

8. S. Sablani, M. Goosen, R. Al-Belushi, and M. Wilf, *Desalination*, 2001, **141**, 269–289.

9. M. Brusilovsky, J. Borden, and D. Hasson, *Desalination*, 1992, **86**, 187–222.

10. S. Lee and C. Lee, *Water Research*, 2000, **34**, 3854–3866.

11. J. Crittenden and M. W. Harza, *Water treatment: principles and design*, John Wiley & Sons, 2005.

12. C. Tzotzi and T. Pahiadaki, *Journal of Membrane Science*, 2007, **296**, 171–184.

13. C. Fritzmann, J. Löwenberg, T. Wintgens, and T. Melin, *Desalination*, 2007, **216**, 1–76.

14. L. F. Greenlee, D. F. Lawler, B. D. Freeman, B. Marrot, and P. Moulin, *Water research*, 2009, **43**, 2317–48.

15. A. G. Pervov, *Desalination*, 1991, **83**, 77–118.

16. M. Okazaki and S. Kimura, *Journal of Chemical Engineering of Japan*, 1984, **17**, 145–151.

17. F. Ahmi and A. Gadri, *Desalination*, 2004, **166**, 427–434.

18. A. Soffer and M. Folman, *Journal of Electroanalytical Chemistry and Interfacial Electrochemistry*, 1972, **38**, 25–43.

19. J. Wu, T. Jiang, D. Jiang, Z. Jin, and D. Henderson, *Soft Matter*, 2011, **7**, 11222–11231.

20. D. Henderson and D. Boda, *Physical chemistry chemical physics : PCCP*, 2009, **11**, 3822–30.

21. M. J. Lochhead, S. R. Letellier, and V. Vogel, *The Journal of Physical Chemistry B*, 1997, **101**, 10821–10827.

22. a. D. Enevoldsen, E. B. Hansen, and G. Jonsson, *Journal of Membrane Science*, 2007, **299**, 28–37.

23. Z. Lazarova and W. Serro, *Separation Science and Technology*, 2002, **37**, 515–534.

24. W. Bowen, R. Kingdon, and H. Sabuni, *Journal of Membrane Science*, 1989, **40**, 219–229.

25. I. Loh, R. Moody, and J. Huang, *Journal of membrane science*, 1990, **50**, 31–49.

26. C. de Lannoy, D. Jassby, K. Gloe, A. D. Gordon, and M. R. Wiesner, *Environmental science & technology*, 2013, **47**, 2760–8.

27. C. de Lannoy, D. Jassby, D. D. Davis, and M. R. Wiesner, *Journal of Membrane Science*, 2012, **415-416**, 718–724.

28. G. Gao and C. D. Vecitis, *Environmental science & technology*, 2011, **45**, 9726–34.

29. W.-Y. Shih, A. Rahardianto, R.-W. Lee, and Y. Cohen, *Journal of Membrane Science*, 2005, **252**, 253–263.

30. N. Cifuentes-Araya, G. Pourcelly, and L. Bazinet, *Journal of Membrane Science*, 2013, **447**, 433–441.

31. M. M. Tlili, M. Benamor, C. Gabrielli, H. Perrot, and B. Tribollet, *Journal of The Electrochemical Society*, 2003, **150**, C765.

32. E. M. Vrijenhoek, S. Hong, and M. Elimelech, *Journal of Membrane Science*, 2001, **188**, 115–128.

33. A. K. Ghosh, B.-H. Jeong, X. Huang, and E. M. V. Hoek, *Journal of Membrane Science*, 2008, **311**, 34–45.

34. S. Khan, M. Al-Shahry, and W. Ingler, *Science*, 2002, **297**, 2243–2245.

35. D. Jiang, D. Meng, and J. Wu, *Chemical Physics Letters*, 2011, **504**, 153–158.

36. M. Kilic, M. Bazant, and A. Ajdari, *Physical Review E*, 2007, **75**, 021502.

37. J. J. López-García, J. Horno, and C. Grosse, *Langmuir : the ACS journal of surfaces and colloids*, 2011, **27**, 13970–4.

Electrochemical Mineral Scale Prevention and Removal on Electrically Conducting Carbon Nanotube – Polyamide Reverse Osmosis Membranes

David Jassby – Corresponding Author

Wenyan Duan – Contact Author

Alexander Dudchenko

Elizabeth Mende

Celeste Flyer

Xiaobo Zhu

Environmental Impact Statement

Mineral scaling is a significant problem in reverse osmosis desalination processes. In this paper we describe how the application of electrical potentials to an electrically conducting carbon nanotube – polyamide composite reverse osmosis membrane can significantly delay the onset of $CaSO_4$ scaling and remove $CaCO_3$ scale from the membrane surface. Thus, the use of electrically conducting reverse osmosis membranes can reduce the use of costly anti-scaling chemicals and eliminate the need for pH adjustments to prevent mineral scale formation.